The Dynamics of Microtubule/Motor-Protein Assemblies in Biology and Physics

Michael J. Shelley

Courant Institute of Mathematical Sciences, New York University, New York, NY 10012; email: shelley@cims.nyu.edu

Annu. Rev. Fluid Mech. 2016. 48:487–506

First published online as a Review in Advance on September 29, 2015

The *Annual Review of Fluid Mechanics* is online at fluid.annualreviews.org

This article's doi: 10.1146/annurev-fluid-010814-013639

Keywords

microtubules, motor proteins, active suspensions, cytoskeleton

Abstract

Many important processes in the cell are mediated by stiff microtubule polymers and the active motor proteins moving on them. This includes the transport of subcellular structures (nuclei, chromosomes, organelles) and the self-assembly and positioning of the mitotic spindle. Little is understood of these processes, but they present fascinating problems in fluid-structure interactions. Microtubules and motor proteins are also the building blocks of new biosynthetic active suspensions driven by motor-protein activity. These reduced systems can be probed—and modeled—more easily than can the fully biological ones and demonstrate their own aspects of self-assembly and complex dynamics. I review recent work modeling such systems as fluid-structure interaction problems and as multiscale complex fluids.

1. BACKGROUND

Through long evolution, nature has engineered subcellular structures that are the scaffolds on which much of the business of life is transacted. This obviously includes the DNA polymer and the cell nucleus, but it also includes the cell and nuclear membranes; other biopolymers such as actin microfilaments, microtubules (MTs), and intermediate filaments; the complex fluidic cytoplasm that fills the cell; and molecular machines (motor proteins) that cross-link, move on, and move subcellular structures.

Biology has long been the inspiration for studying how actively driven structures interact with fluids, with the flight of birds and swimming of fish as classical examples. However, the microcosm of the cell provides other, less easily observed, but equally fascinating instances. **Figure 1** illustrates some of the events leading to the first cell division in a *Caenorhabditis elegans* embryo. **Figure 1*a–c*** shows the migration and positioning of the pronuclear complex (PNC), which carries the male and female genetic material to the center of the cell. However this process might be effectuated, the proper positioning and orientation of the complex, and thus that of the subsequent mitotic spindle (**Figure 1*c–e***), are crucial for asymmetric cell division and the generation of cell diversity during development. Pronuclear positioning is a daunting problem in fluid-structure interactions as the PNC is itself geometrically complex given its association with two dense arrays of stiff biopolymers—MTs—which are themselves involved in driving the complex through the cytoplasm. **Figure 1*d,e*** captures another fluid-structure interaction as chromosome copies are divided and are then moved to opposite ends of a cell before cell division (**Figure 1*f***).

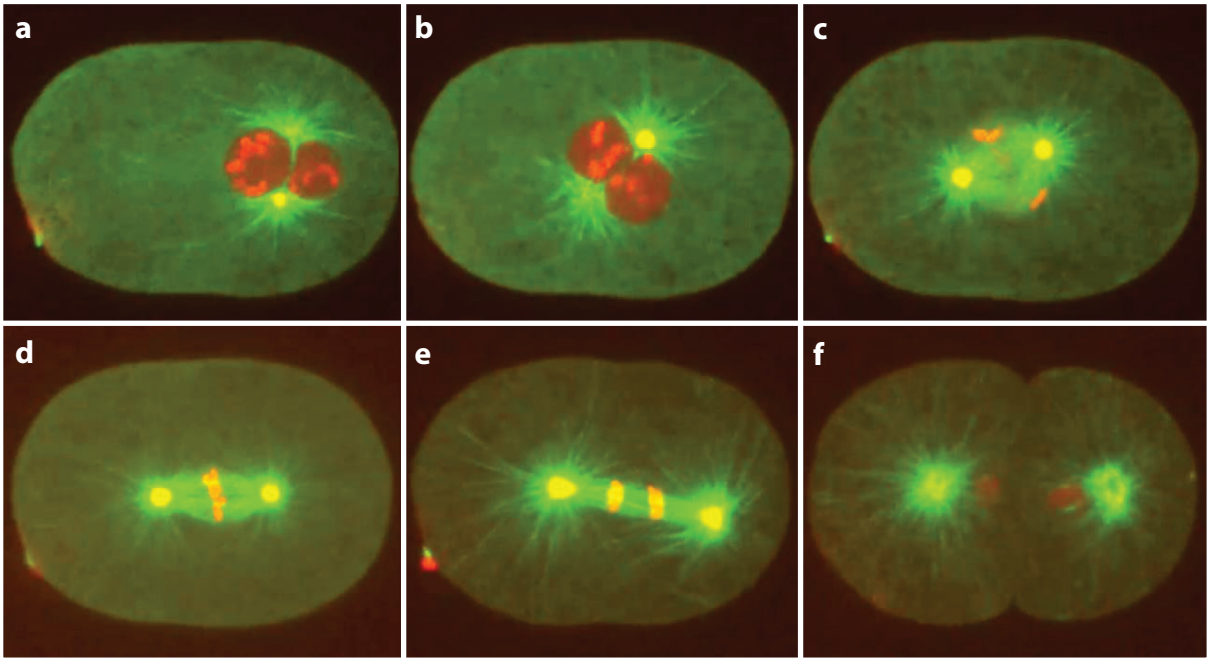

Figure 1

Snapshots of different stages of the first cell division in a single-cell *Caenorhabditis elegans* embryo: (*a–c*) pronuclear centering and rotation, (*c,d*) spindle formation, (*e*) asymmetric spindle elongation and chromosome segregation, and (*f*) cell division. Here tubulin is labeled with a green fluorescing molecule, and the chromosomes are labeled with a red fluorescing molecule. Figure modified with the permission of Asako Sugimoto.

Centrally involved in all of these processes—pronuclear migration, mitotic spindle formation, chromosome segregation—are MTs, which are the stiffest of the subcellular biopolymers. They have a polar structure with plus ends and minus ends and are quite dynamic, substantially changing their lengths through polymerization and depolymerization. MTs interact with each other, and with immersed structures within the cell, through the mechanical coupling of motor proteins, direct mechanical contact, and the flows that their motions create. MTs are an essential part of the cell's cytoskeleton.

Because of their biological importance, the interaction of MTs and motor proteins has been studied in vitro. Experiments have shown the formation of a wide variety of steady-state structures, including asters, which are reminiscent of the centrosomal array (Nédélec et al. 1997, Surrey et al. 2001, Schaller et al. 2010). Other recent experiments have combined stabilized MTs with synthetic agents, such as depletants, to create biosynthetic suspensions. When driven by internal motor-protein activity, these suspensions can demonstrate the self-assembly of dynamic structures, such as MT assemblies that exhibit a ciliary-like beating and coordination (Sanchez et al. 2011), and condensed active liquid-crystalline surface states (Sanchez et al. 2012), whose dynamics are similar to those observed in dense suspensions of motile bacteria (Cisneros et al. 2011).

All of these MT-related phenomena, from pronuclear positioning to engineered active suspensions, are examples of active matter in which the macroscopic dynamics are driven by a microstructure that converts a local source of energy, usually chemical, into a change in the microstructure conformation. This review focuses on the hydrodynamics of assemblies of immersed MTs and driving motor proteins, which fuel their motion through ATP hydrolysis. At the level of individual MTs, we are essentially studying long and slender elastic rods, immersed within a fluid, on which motor proteins move in preferential directions and couple them to other MTs or structures. At the ensemble level, we are considering complex, ordered fluids whose dynamics are driven by the internal stresses created by motor-protein activity and MT displacement. For reviews on the related subject of active actin-myosin gels, readers are referred to Juelicher et al. (2007) and Prost et al. (2015).

2. SOME BASIC INGREDIENTS

2.1. Microtubules and Their Dynamics

MTs are polymers composed of tubulin dimers, with each dimer comprising an α- and β-tubulin protein molecule. These dimers polymerize into a cylindrical shell, with an outer diameter of approximately 24 nm, that surrounds a hollow core. The dimer shell has a chirality that gives MTs an intrinsic directionality, or polarity. Thus, one end of an MT can be labeled the plus end, and the other the minus end. The flexural rigidity, B_{MT}, of taxol-stabilized MTs has been measured in vitro to be approximately 10^{-23} N m^2 (Gittes et al. 1993)—that for unstabilized MTs is somewhat less (Mickey & Howard 1995)—which is over two orders of magnitude larger than that measured for actin filaments, and which corresponds to a persistence length of over 10^3 μm, well above cellular dimensions.

MTs are highly dynamic and, unless stabilized, will successively polymerize and depolymerize in a process termed dynamic instability (Mitchison & Kirschner 1984, Desai & Mitchison 1997), with transitions between these states termed catastrophe (growing to shrinking) and recovery (shrinking to growing). Polymerization (depolymerization) typically takes place at the plus end through the addition (removal) of dimer subunits (**Figure 2*a***, parts i and ii, respectively). Typical polymerization and depolymerization speeds and catastrophe and recovery rates can be found in Kimura & Onami (2005). Average MT lifetimes in vivo are less than 1 min, whereas processes

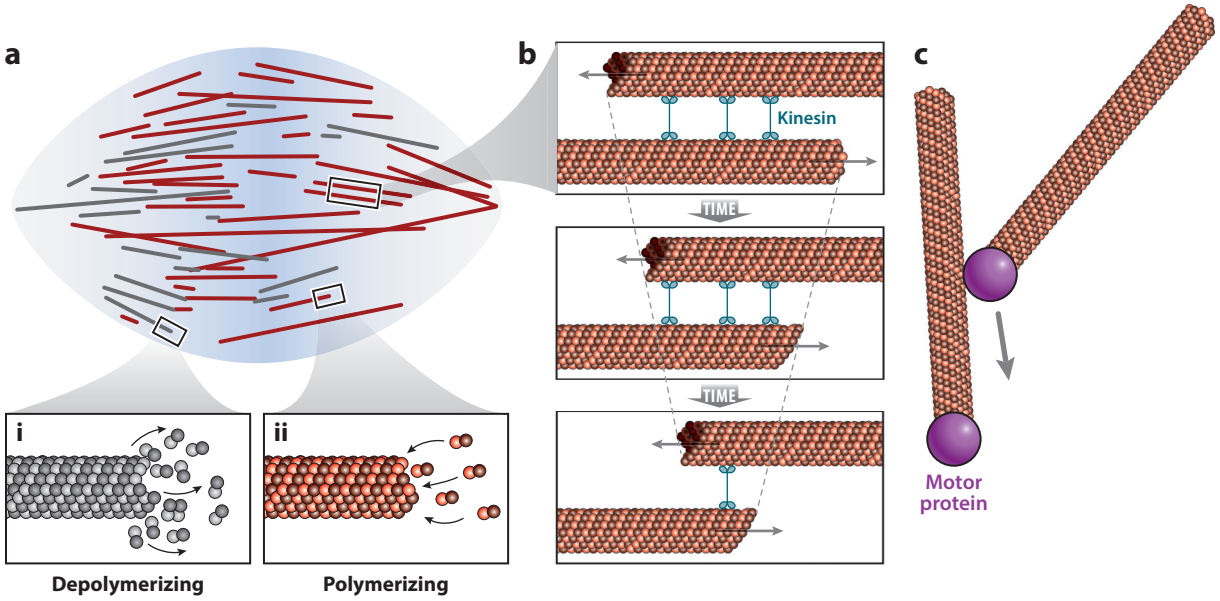

Figure 2

Conceptual model of spindle organization. (*a*) Aligned microtubules (MTs) are both polymerizing (*red*) and depolymerizing (*gray*). (*i*) MTs depolymerize by losing dimer subunits from their plus ends and (*ii*) polymerize by adding dimer subunits at their plus ends. (*b*) Multiheaded kinesin complexes (*aqua*), which are plus-end directed, walk along MTs of opposing polarity (indicated by *arrows*). These MTs slide past each other toward their minus ends. This process is called polarity sorting (Nakazawa & Sekimoto 1996). Panels *a* and *b* reproduced with permission from Brugués et al. (2012). (*c*) Schematic illustration of the minus end of an MT being pulled down toward the minus end of another MT by a minus-end-directed dynein motor protein (*purple*).

such as pronuclear migration and spindle assembly and maintenance can take 10–30 min or more.

2.2. Motor Proteins

Important to this review are motor proteins that walk along MTs, particularly kinesins and dyneins. One important difference between dynein and kinesin is that although both are end directed, kinesins walk toward the MT plus end, and dyneins walk toward its minus end. These directed motions are often associated with the motion of objects in the cell. An example involves multiheaded kinesin complexes thought to cross-link nearby MTs within the mitotic spindle (Saunders & Hoyt 1992) (**Figure 2*a*,*b***). Given that they are end directed, if two such cross-linked MTs are anti-aligned (with plus ends pointing in opposite directions), the opposing motion of the motor heads leads to MTs sliding past one another. This process is termed polarity sorting (Nakazawa & Sekimoto 1996) and is associated with MT dynamics within the spindle (Brugués et al. 2012). A related MT transport process is the conjectured clustering of MT minus ends by dynein walkers (Verde et al. 1991) (**Figure 2*c***).

Another important example involves the transport of cargo along the cytoskeleton; for example, yolk granules suspended within the cytoplasm are transported along MTs by dyneins bound to the surface of granules (as discussed in the next section) (**Figure 3**). The speed of motor-protein walking is a function of the load, for example, that produced by hydrodynamic drag of their cargo, and the relationship between speed and load has been much studied (Visscher et al. 1999). In short,

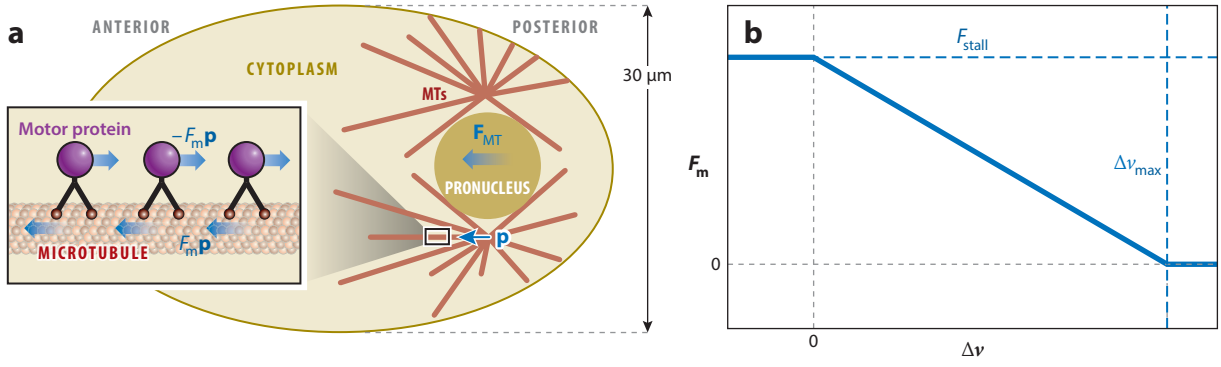

Figure 3

Schematic illustration of the biophysical model of Shinar et al. (2011), inspired by Kimura & Onami (2005). (*a*) An ellipsoidal cell boundary encapsulating the cytoplasm (*yellow*), pronucleus (*dark yellow*), and associated microtubules (MTs) (*red*). Asymmetric lengths of MTs due to growth cessation at the cortex create a force imbalance $\mathbf{F}_{MT}$ favoring centration. (*Inset*) Motor proteins (*purple*) embedded in the cytoplasm exert equal and opposite forces, $\pm F_m\mathbf{p}$, on the cytoplasm and MT, resulting in their relative motion. (*b*) The relationship between load F_m and velocity Δv for a single motor protein. Figure adapted with permission from Shinar et al. (2011).

retarding loads slow the motor protein, with the speed becoming zero at the stall force, F_s, which is on the order of 1 pN. Expediting loads are typically resisted by the motor protein, leading to little change in speed.

It is noteworthy that a 1-pN load is easily enough to significantly bend or buckle an MT. This can be seen by considering $R = F_s/(B_{MT}/L^2)$, the ratio of stall force to a characteristic MT elastic force. For an MT of 8-μm length, this gives $R \approx 7$.

2.3. The Cytoplasm

By definition, in vivo experiments take place within the cell, and the complex liquid that fills it is termed the cytoplasm. The cytoplasm is approximately 80% water, with the remaining 20% including many types of soluble proteins and various small suspended structures, such as membrane-bound organelles and yolk granules. Many in vitro experiments actually utilize extracted and purified cell cytoplasm as this preserves much of the molecular machinery needed for the assembly of structures such as spindles.

The mechanical properties of the cytoplasm are complex. Recent modeling and measurements of cytoplasmic response in living cells suggest that the cytoplasm is best conceived of as a poroelastic material (Moeendarbary et al. 2013). Other studies suggest that this may depend on the cell type and developmental stage. Using particle tracking microrheology, Daniels et al. (2006) found that the cytoplasm of the much-studied single-cell *C. elegans* embryo responds as a very viscous Newtonian liquid, with a viscosity approximately 1,000 times that of water. Of course, rheological responses can be scale dependent, and given the complexity of the cytoplasm, many modeling studies have simply assumed a Newtonian response (Kimura & Onami 2005, Niwayama et al. 2011, Shinar et al. 2011).

3. NATURAL ASSEMBLIES OF MICROTUBULES AND MOTOR PROTEINS

The most-studied natural assemblies of MTs and motor proteins are the centrosomal array and the mitotic (and meiotic) spindle. The centrosomal array is a collection of MTs that are nucleated

from so-called centrosomes, or MT organizing centers. The centrosome is a small organelle whose composition remains an object of study (Mardin & Schiebel 2012). The minus ends of centrosomal MTs are contained within the centrosome, whereas the plus ends grow into the cellular cytoplasm, making contact with the cell cortex and chromosomes (**Figure 1**). The centrosomal array of MTs is thought to be involved in both the positioning of the mitotic spindle and chromosome segregation (McIntosh et al. 2012).

The mitotic spindle is a self-assembled structure within the cell composed of MTs, cross-linking proteins, and motor proteins (McIntosh et al. 2012). In vivo, mitotic spindles are thought to form through MT nucleation following the dissolution of the nuclear membrane (Brugués et al. 2012). Spindles can be highly ordered, with MTs in an aligned liquid-crystalline state (Brugués & Needleman 2014). The MTs within the spindle are constantly overturning through dynamic instability, having lifetimes on the order of 1 min, whereas the spindle is itself assembled and maintained on the order of 1 h (Brugués & Needleman 2014). With the assembly of the mitotic spindle, chromosomes in a condensed state are positioned in the midplane of the spindle, and copies are divided and segregated to opposite ends of the cell. The precise mechanics by which this takes place are yet to be determined. Spindles can be spontaneously formed in vitro by adding genetic material to cell extracts (Heald et al. 1996). Such spindles can be stabilized for hours, whereas again their MT constituents overturn in less than 1 min. They also show great robustness under experimental perturbation. For example, spindle self-healing after laser ablation has been used to deduce MT length distributions (Brugués et al. 2012).

3.1. Modeling and Simulations of Flow and Transport

There are several aspects to the modeling of MT/motor-protein assemblies. One is to describe the basic mechanics of an MT under external loads. The simplest nontrivial approach is to simply consider the MT as a rigid rod or as a simple Euler beam. The former is appropriate for short MTs, such as those used in the experiments of Sanchez et al. (2012), whereas the latter is appropriate for longer MTs, such as those that span the mitotic spindle or that compose the centrosomal array. Another aspect is the way in which an MT interacts with the surrounding medium. Most if not all studies to date have described that medium as being a very viscous Newtonian fluid.

Discrete structure models have been used to study many elements of MT/motor-protein interactions. One popular and influential modeling tool is Cytosim (Nédélec & Foethke 2007), which is a software package for evolving immersed mechanical structures such as flexible fibers, spheres, and other objects. Inertia is considered as negligible, and although thermal fluctuations and local drag forces are accounted for, long-ranged fluid flows are not. Cytosim has been used to simulate the self-assembly of MT arrays in fission yeast (see Nédélec & Foethke 2007 for a review), to construct a computational model of the *Xenopus* meiotic spindle (Loughlin et al. 2010), and recently to investigate the ability of slender spindles to resist compressive loads (Ward et al. 2015).

The interaction of elastic fibers with fluid flows is a type of fluid-structure interaction for which specialized mathematical descriptions and computational methods have been developed. The most basic and easy to use of these is local slender-body theory, which gives a local anisotropic relation between elastic and drag forces. Nonlocal hydrodynamic interactions can be captured through the use of higher-order, more complex, slender-body formulations (Tornberg & Shelley 2004) or through other approaches, such as immersed boundary methods (Peskin 2002, Nguyen & Fauci 2014), bead-rod models (Hämäläinen et al. 2011), or regularized Stokeslet methods (Olson et al. 2013). These methodologies and their applications to understanding fluid-structure interactions, such as buckling instabilities at low Reynolds numbers, have recently been reviewed (Lindner & Shelley 2015).

The effect and nature of cytoplasmic flows have been studied for pronuclear positioning in embryonic cells. As discussed in Section 1, **Figure 1*a*** shows, for the single-celled *C. elegans* embryo, the cell's PNC, which comprises the fused male (posterior, or right side) and female (anterior, or left side) nuclei. Also shown in the figure are the two MT arrays that nucleate from the two centrosomes. As seen in **Figure 1*a–c***, the complex moves toward the center of the roughly ellipsoidal cell while simultaneously rotating so that the centrosomes are aligned with the long axis. This is sometimes referred to as proper positioning. This positioning precedes the formation of the mitotic spindle (**Figure 1*d***), which is followed by chromosome segregation (**Figure 1*e***) and cell division (**Figure 1*f***).

The biophysics underlying nearly every step of this process are ill understood, including how the PNC first moves into the proper position. Hypotheses on how the proper position is achieved invoke MTs pushing against the cell periphery (Reinsch & Gonczy 1998) and the pulling action of force generators—other motor proteins—at the cell periphery (Grill et al. 2001). Kimura & Onami (2005) posited that motor proteins immersed in the cytoplasm, perhaps anchored to mobile payloads, attach themselves to centrosomal MTs and pull or tow the complex to the cell center. In this scenario, if the PNC is off-center, then MTs will on average grow longer toward the center. It is known that minus-end-directed dyneins attach to MTs and tow payloads toward the associated centrosome. This should generate a pulling force on the MT toward its free plus end. Longer MTs can anchor more motor proteins and hence will generate a mean pulling force toward the center.

Kimura & Onami (2005) computationally modeled the PNC as a sphere that experiences a simple Stokes drag generated by length-dependent, plus-end-directed pulling forces on attached centrosomal MT arrays. The model MTs themselves depolymerize on contact with an ellipsoidal shell. Although this simple model ignores the fluid flows generated by MT motion, the motion of the motor-protein payloads, and the confinement of cytoplasmic flow afforded by the cell periphery, it does show how centering might be achieved by MT growth asymmetry.

Shinar et al. (2011) re-examined the conceptual model of Kimura & Onami (2005) within a more realistic computational framework that incorporated the cytoplasmic flows generated by (*a*) payloads carried along MTs by motor proteins obeying a velocity-load relation, (*b*) the motion of the PNC, and (*c*) the presence of the egg shell on which a no-slip condition is imposed (**Figure 3**). For simplicity, and in agreement with microrheological studies of *C. elegans* embryos (Daniels et al. 2006), it was assumed that the cytoplasm was a Newtonian fluid with a viscosity μ that is 10^3 times that of water (1 cP). This model was instantiated in an immersed boundary framework in which constraint forces on the fluid are determined on all boundaries (PNC, MTs, cell periphery) to satisfy the appropriate boundary conditions. In particular, the cytoplasmic fluid obeys the forced Stokes equation

$$\nabla \cdot \Sigma = \mu \Delta \mathbf{u} - \nabla q = -\mathbf{g}_{\mathrm{MT}} \quad \text{and} \quad \nabla \cdot \mathbf{u} = 0, \tag{1}$$

where $\Sigma = -q\mathbf{I} + \mu(\nabla \mathbf{u} + \nabla \mathbf{u}^T)$ is the Newtonian stress tensor, and $\mathbf{g}_{\mathrm{MT}}$ is the Eulerian MT-based force density driving the flow. Let us consider a single MT with orientation vector $\mathbf{p}$ and centerline coordinate $\mathbf{X}_{\mathrm{MT}}(s, t)$, with the arc length s measured from the centrosome-bound minus end. In this model, as in that of Kimura & Onami (2005), motor proteins move along the MT, transporting cargo while exerting a pulling force on the MT and its associated structures. The force density at distance s along the MT is given by $\mathbf{G}_{\mathrm{MT}}(s) = DF_{\mathrm{m}}(s)\mathbf{p}$, where D (taken as constant) is the density per unit length of motor proteins, F_{m} is the force exerted on the MT by a single motor protein, and $\mathbf{p}$ is the direction of that force (along the MT). Here F_{m} obeys a velocity load relation (see Shinar et al. 2011) (**Figure 3**). The total MT-based force and torque on the attached PNC, with

center $\mathbf{X}_0(t)$, are then

$$\mathbf{F}_{MT} = \int_{MT} ds\, \mathbf{G}_{MT}(s) \quad \text{and} \quad \mathbf{T}_{MT} = \int_{MT} ds\, (\mathbf{X}(s) - \mathbf{X}_0) \times \mathbf{G}_{MT}(s), \tag{2}$$

and hence we must have

$$\mathbf{F}_{MT} + \int_{\partial PNC} dS\, \boldsymbol{\Sigma} \cdot \mathbf{n} = \mathbf{0}, \tag{3}$$

$$\mathbf{T}_{MT} + \int_{\partial PNC} dS (\mathbf{x} - \mathbf{X}_0) \times \boldsymbol{\Sigma} \cdot \mathbf{n} = \mathbf{0}. \tag{4}$$

where ∂PNC denotes the surface of the PNC, and $\mathbf{n}$ is its outward normal. The same motor-protein motion also generates an equal and opposite force on the fluid along the MT, having the Eulerian force density

$$\mathbf{g}_{MT}(\mathbf{x}, t) = -\int_{MT} ds\, \delta(\mathbf{x} - \mathbf{X}(s, t))\mathbf{G}(s, t). \tag{5}$$

In this fashion, motor-protein pulling forces are communicated to the fluid, generating streaming flows along MTs toward the PNC, as indeed observed during centering (Shinar et al. 2011). Within the immersed boundary framework, no-slip boundary conditions on the cell periphery and the PNC are enforced by the determination of a constraint force in a fashion reminiscent of the distributed Lagrange multiplier method of Glowinski et al. (1999).

The process of dynamic instability is also simulated within the model, in which MTs grow and shrink stochastically. MTs are also assumed to be rigid and to depolymerize (undergo catastrophe) on contact with the cell periphery.

Figure 4 shows a simulation of this model in which the PNC begins on the posterior of the cell (Shinar et al. 2011). Given the PNC's proximity to the periphery, MTs grow longer anterior-wise, and cytoplasmic pulling forces tow the PNC leftward. This is unsurprising, but what is most interesting is that the complex then begins a rotation that terminates in the proper position, that is, with the alignment of the centrosomes along the anterior-posterior axis. This rotation arises naturally in this model because of the ellipsoidal shape of the embryo, which allows a torque-driven instability. If the centrosomes are lined up orthogonally to the anterior-posterior axis, then slight rotational perturbations allow MTs that are nearly tangential to the PNC to grow longer in the direction of rotation. This induces a torque that drives the rotation further. **Figure 4*d–f*** also shows the streamlines of the flow, demonstrating that at early times, the PNC is essentially a puller swimmer (Saintillan & Shelley 2013) moving in confined space. Confinement also increases the active forces necessary to center the PNC on reasonable timescales, increasing the necessary motor-protein forces by an order of magnitude relative to Kimura & Onami's (2005) model. This model has gained support from the knockdown experiments of Kimura & Kimura (2011), who showed that centering was significantly impaired by inhibiting the attachment of dynein motor proteins to mobile organelles.

Although the model is elaborate and physically realistic in many aspects, it suffers from some shortcomings. First, the MTs are assumed to be rigid even though the forces associated with motor proteins are sufficient in principle to bend them. Second, the number of MTs that can be simulated is modest, $O(50)$, because of the constraints of the numerical method. Relatedly, although the MTs "exert" an active tangential force on the fluid (through our model of motor protein forcing), they themselves experience no transverse drag as this would require substantially more numerical resolution. This suggests that the model may substantially underestimate the total system drag. The ratio r_D of the Stokes drag on a sphere of radius a to that on a slender rod of length $2a$ (Tornberg & Shelley 2004), with both moving at the same speed, is approximately

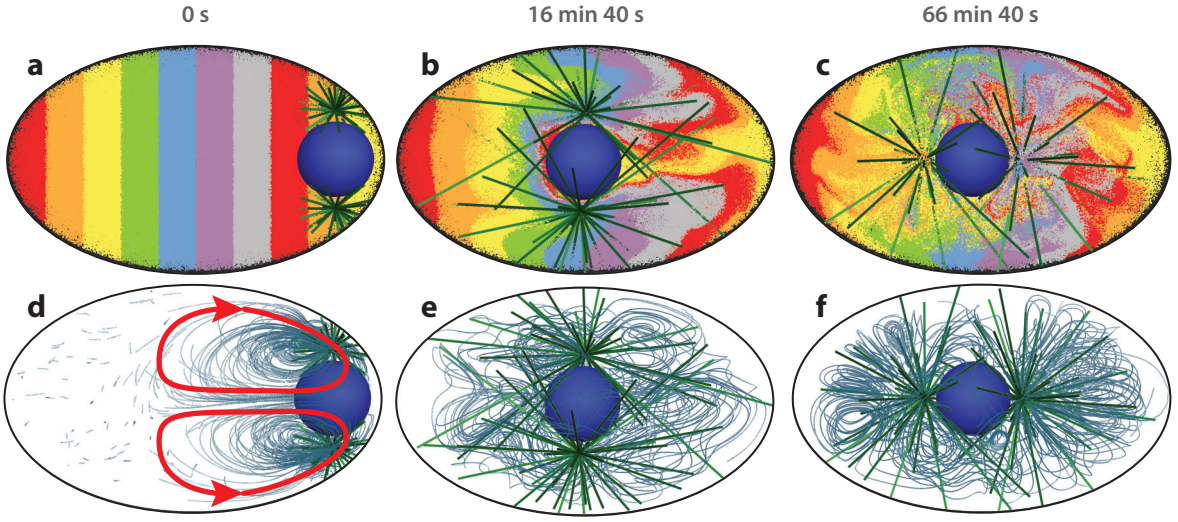

Figure 4

The full simulation of Shinar et al.'s (2011) model. (*a*,*d*) The pronuclear complex (PNC) starts at the posterior axis. (*b*,*e*) Asymmetric microtubule (MT) lengths due to cessation of MT growth at the cortex lead to centration of the PNC. (*c*,*f*) Fluctuations in the MT lengths initiate a rotation of the PNC, which continues until it is aligned with the anterior-posterior end of the cell. Panels *d–f* additionally show streamlines of the cytoplasmic flow. Figure adapted with permission from Shinar et al. (2011).

$r_D = (3/8)(-\ln \epsilon^2 e)$, where ϵ is the aspect ratio of the MT. With $a = 2.5$ μm (the scale of a *C. elegans* pronucleus), a single MT already has a drag 25% that of the sphere. Of course, drag will not scale linearly with the number of MTs as they may collectively carry the same volume of fluid as would only a few.

This problem is currently being revisited within a much more flexible framework while staying within (and exploiting) the constraints of a Newtonian cytoplasm. **Figure 5** shows the results of two simulations (E. Nazockdast, A. Rahimian, D.J. Needleman & M.J. Shelley, manuscript in preparation) investigating different models of positioning in which, as in **Figure 4**, the PNC begins near the posterior side of the cell. For the model in **Figure 5*a***, there are no motor proteins; instead, polymerizing MTs can exert pushing forces on the cell periphery, moving the PNC to the center of the cell (Reinsch & Gonczy 1998). For the biophysical parameters used in this simulation, rotation of the PNC into the proper orientation occurs but only very slowly (in this late-time snapshot, the PNC is not yet in the proper position). Because MTs are flexible, the pushing forces at the periphery can also buckle the MTs, as is evident. The simulation in **Figure 5*b*** uses the cytoplasmic pulling model of Shinar et al. (2011) but with the MTs now fully coupled to the flow, thus accounting for transverse drag forces and allowing for MT flexibility. This late-time snapshot shows that the PNC has migrated to the center and has rotated into the proper position. MTs show very little bending as the cytoplasmically bound force generators typically exert extensile stresses on them.

Here the Stokes equations are solved within a boundary integral formulation in which all of the discrete structures—the PNC, MTs, cell periphery—are represented explicitly. MTs are modeled as elastic beams that can bend under applied loads and the drag from fluid flows, and they themselves move fluid as they move. Within a boundary integral formulation of the Stokes equations (Pozrikidis 1992), only the surfaces of immersed structures are resolved numerically, not the fluid volume, and these surfaces communicate through convolution integrals whose kernels are formed from fundamental solutions of the Stokes equations. This amounts to a reduction in

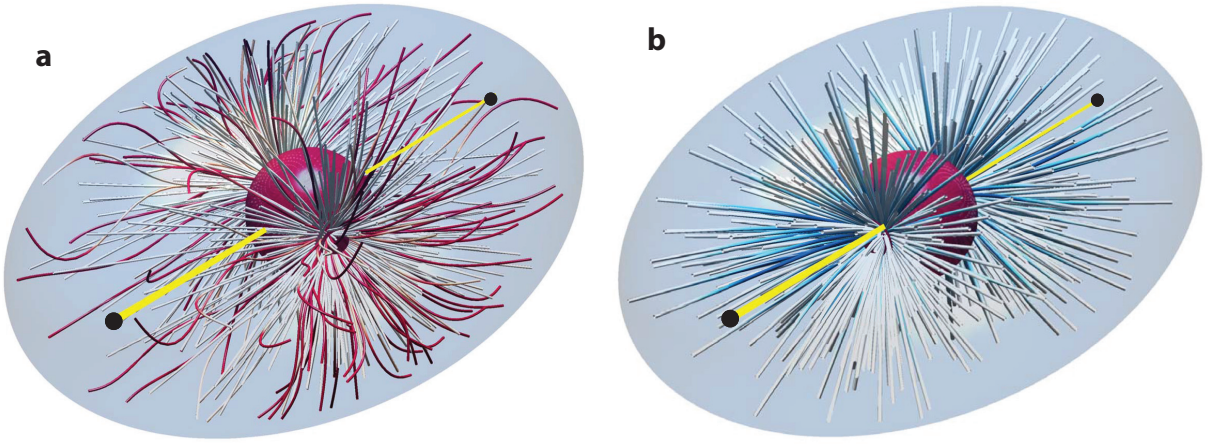

Figure 5

Simulations of pronuclear migration with hydrodynamic interactions between microtubules (MTs), the pronuclear complex (PNC), and cortex using nonlocal slender-body theory and a boundary integral formulation (E. Nazockdast, A. Rahimian, D.J. Needleman & M.J. Shelley, manuscript in preparation). (*a*) Polymerization forces from the cell cortex center the PNC and induce strong MT buckling near the cortex. PNC rotation is not achieved until 30 min after PNC formation, whereas the positioning occurs in roughly 10 min in wild-type embryos. (*b*) Cytoplasmic pulling forces from immersed dynein motors can properly position the PNC after 11 min of PNC formation. The MTs are under extensile forces and thus are relatively straight. For both simulations, the number of fibers is $N_{\mathrm{MT}} = 576$. The parameters given by Kimura & Onami (2005) are used. The MTs are color coded according to the local tension on them; red, blue, and white correspond to compressive, extensive, and zero tension forces, respectively.

the computational dimensions from three to two and allows the use of fast-multipole methods (Greengard & Rokhlin 1987) for the resulting many-body problem.

Briefly, the contribution of MTs to the boundary integral formulation is a nonlocal slender-body expression that reduces a single-layer surface integral to a line integral along the MT centerline (Keller & Rubinow 1976, Tornberg & Shelley 2004). The contributions from the cell periphery and PNC surface are expressed through the double-layer formulation of Power & Miranda (1987), which requires the solution to a second-kind integral equation for an unknown double-layer surface density. The bending response of the MTs, described by the Euler-Bernoulli elasticity, makes their evolution temporally stiff, and Nazockdast et al. used implicit time integration methods related to those developed by Tornberg & Shelley (2004) for evolving suspensions of flexible fibers (E. Nazockdast, A. Rahimian, D.J. Needleman & M.J. Shelley, manuscript in preparation). Each time step requires the solution of a large system of linear equations for updated MT positions, MT axial tensions that enforce MT inextensibility, and double-layer surface densities. This is done within a GMRES iteration (Saad & Schultz 1986) with specialized preconditioners, with fast matrix-vector multiplications performed using a generalized kernel version of the fast-multipole method for the Stokes equations (Ying et al. 2004). In short, this simulation captures the full set of hydrodynamic interactions at a linear cost in the number of unknowns and with no high-order time-step constraints.

Perhaps such fluid-structure simulations will help reveal the operative mechanisms in transport processes such as PNC positioning. This may be possible given that different mechanisms have different cytoplasmic flow signatures, which can be investigated numerically. This effort may be complicated by the strong possibility that more than one mechanism is at play in positioning the PNC (Kimura & Onami 2007, Kimura & Kimura 2011).

3.2. Some Related Work

The cytoplasmic pulling model gives streaming flows along MTs toward the centrosomes (Shinar et al. 2011). Cytoplasmic streaming is observed in many other contexts. For example, in the very early stages of pronuclear migration in the *C. elegans* embryo, the female pronucleus moves from the anterior side toward the male pronucleus, presumably because of streaming flows along the cell periphery (Hird & White 1993) produced by motions of the actin-myosin cortex. This is an excellent fluid-structure problem in its own right, and the nature of these streaming flows has been investigated experimentally and theoretically (Niwayama et al. 2011). Goldstein and collaborators (Verchot-Lubicz & Goldstein 2010, Ganguly et al. 2012, Woodhouse & Goldstein 2013) recently investigated and modeled several aspects of cytoplasmic streaming induced by motor proteins moving along cytoskeletal elements.

4. BIOSYNTHETIC ASSEMBLIES

Mixtures of MTs and motor proteins have been extensively studied outside of the cell, with early experiments showing static self-organized structures, such as vortices (which refer to the MT patterning and not necessarily to fluid flows) and asters, with the latter reminiscent of the centrosomal array. **Figure 6** shows experimental examples from seminal works of asters formed from MTs and multiheaded kinesin complexes (**Figure 6*a***; Nédélec et al. 1997) and vortices found in gliding assays of MTs driven by surface-bound dyneins (**Figure 6*b***; Sumino et al. 2012). This pattern-forming system has been extensively reviewed by Vignaud et al. (2012).

Recently, the laboratory of Z. Dogic synthesized relatively simple mixtures of micrometer-scale MTs (stabilized against dynamic instability) with synthetic multiheaded kinesin complexes and an additional depletant agent (PEG) that promotes MT bundling. Relative to the more disperse systems discussed above, in this system bundling greatly increases the probability of MT interactions through motor-protein coupling. In the presence of ATP, walking motor proteins can induce relative sliding between MTs of opposite polarity (i.e., polarity sorting).

For bundles attached to a surface, Sanchez et al. (2011) demonstrated that such bundles show oscillatory, ciliary-like collective beating (**Figure 6*c***) and that arrays of such bundles could produce metachronal wave patterns reminiscent of those seen in dense fields of cilia. The oscillatory motion presumably follows from sliding of antipolar MTs within the bundles, induced by multiheaded kinesin complexes. As yet, no quantitative model has been put forward that investigates this possibility.

In the bulk, Sanchez et al. (2012) showed that such MT bundles stretched, fractured, and merged with each other (**Figure 6*d***). Their stretching presumably again reflects tethered kinesin complexes walking on anti-aligned MTs, inducing antiparallel sliding. Fracturing likely occurs at points where polarity sliding has produced a domain boundary, devoid of MTs, between antipolar regions. At high MT concentrations, these bundles form a dynamic network whose stretching and fracturing create fluid flows, and as measured by particle tracking, these flows have velocity magnitudes that scale with the ATP concentration but whose spatial correlation lengths are relatively independent. This seems consistent with the bundle network having reached the analog of an overlap concentration in which the length is determined by the development of strong interactions with neighboring bundles. There is not yet a theoretical model that predicts these correlation lengths or the nature of the bulk flow fields.

The dynamics are quite different when MT bundles are adsorbed onto an oil-water interface (**Figure 6*e***). There they instead form a dense, nematically ordered surface state characterized by complex and time-dependent surface flows, and the spontaneous and continual generation and

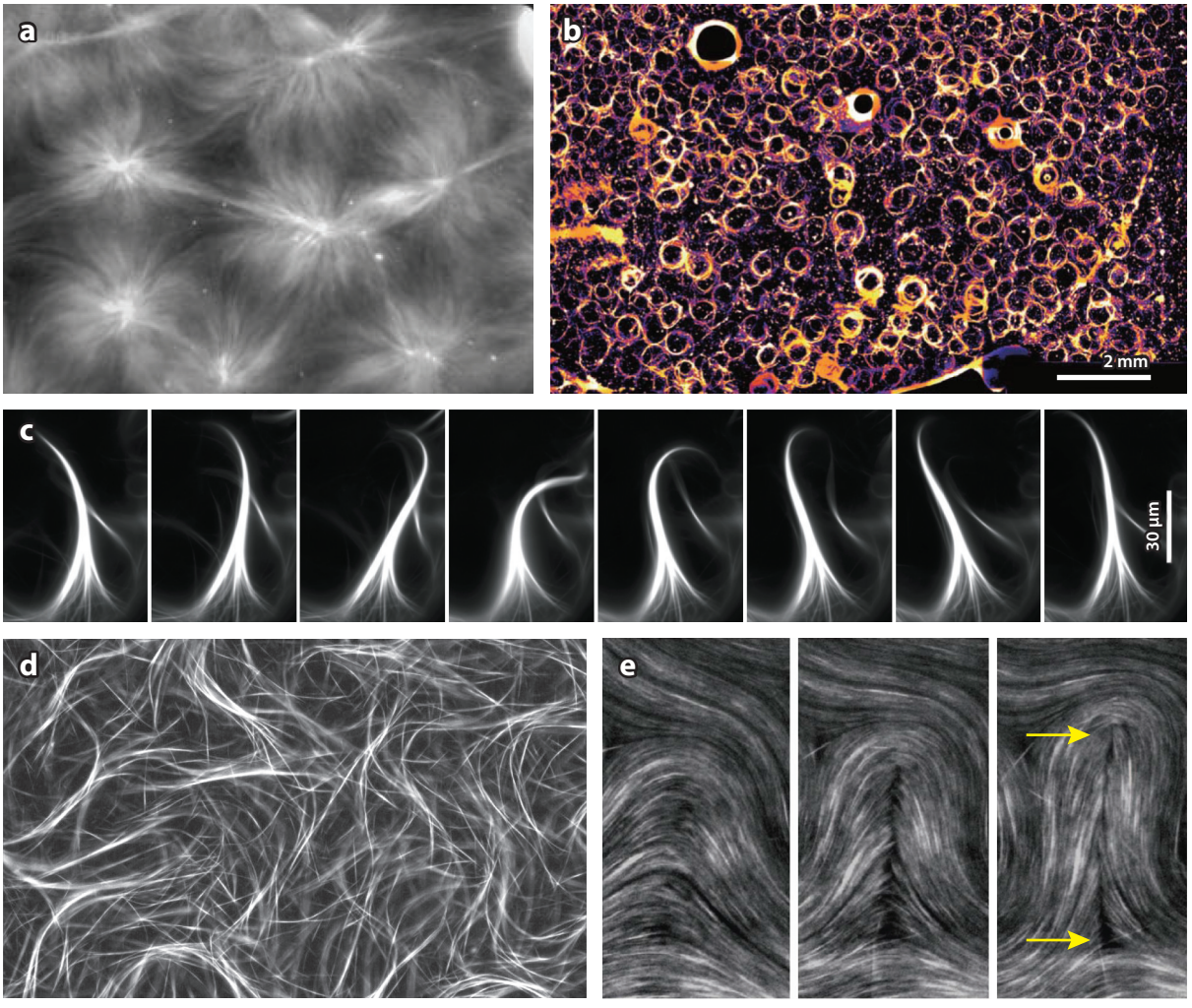

Figure 6

In vitro assemblies of microtubules (MTs) and motor proteins. (*a*) Aster patterns formed from MTs and kinesin motor-protein complexes. Panel *a* taken with permission from Nédélec et al. (1997). (*b*) MT vortices formed in gliding assays of MTs driven by surface-bound dyneins. Panel *b* taken with permission from Sumino et al. (2012). (*c*) Ciliary-like beating of MT clusters bound to a surface, driven by kinesin complexes. Panel *c* taken with permission from Sanchez et al. (2011). (*d*) The formation of MT clusters in bulk that stretch, merge, fracture, and produce complex fluid flows. Panel *d* taken with permission from Sanchez et al. (2012). (*e*) Snapshots of an active liquid-crystalline state of dense MT bundles bound to an immersed surface, showing the birth and separation of a disclination singularity pair of order $\pm 1/2$ (indicated by the *upper* and *lower yellow arrows*, respectively).

annihilation of disclination defect pairs, of $\pm 1/2$ order, in the MT orientation field (Sanchez et al. 2012). The topological structure of the orientation field was recently investigated, both experimentally and theoretically, for spherical droplets with active MT surfaces (Keber et al. 2014).

Inspired by the active surface experiments of Sanchez et al. (2012), both Giomi et al. (2013, 2014) and Thampi et al. (2013, 2014) studied liquid crystal hydrodynamic models with fluid flow driven by an apolar active stress (Simha & Ramaswamy 2002). Although these rather general models reproduce aspects of the experiments, the microscopic origins of the driving active stresses

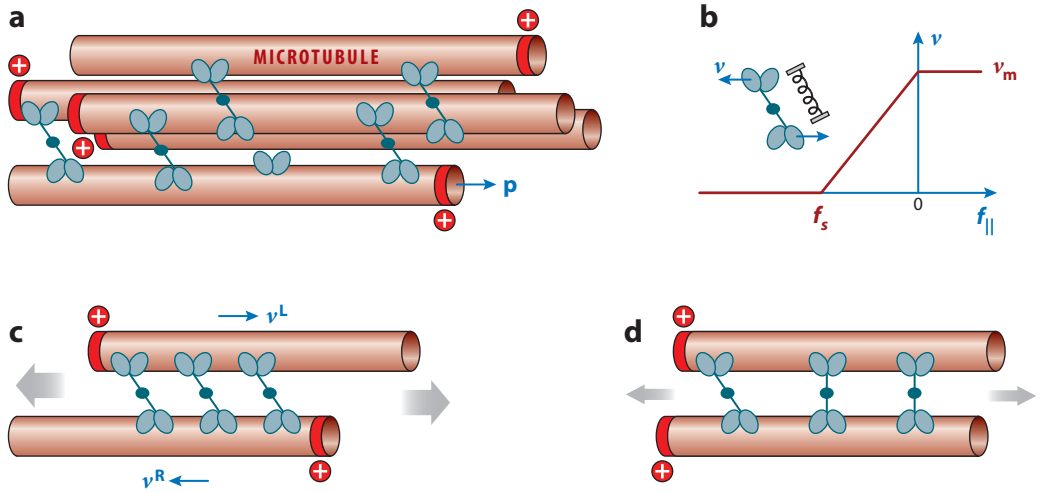

Figure 7

(*a*) Schematic illustration of a cluster of polar-aligned and anti-aligned microtubules (MTs), with plus ends marked by red rings. Motors walk on neighboring MTs. (*b*) Spring-like forces exerted on neighboring MTs by motors. (*c*) An anti-aligned MT pair. (*d*) A polar-aligned MT pair. Gray arrows characterize the magnitude of the extensile stress. Figure adapted with permission from Gao et al. (2015).

are unexplained, as is the role, if any, played by MT polarity. Interactions between MTs and motor proteins are inherently polar. Gao et al. (2015) constructed a multiscale model built on the directional translocation of motors along MTs that captures polar-specific interactions and identifies possible sources of destabilizing active stresses.

Figure 7 outlines the basic physical picture. Each polar MT has a plus-end-oriented director **p**, a length l, and diameter b (**Figure 7*a***). Nearby MTs are coupled by active plus-end-directed cross-links consisting of two motors connected by a spring-like tether (**Figure 7*b***). Motor velocities along an MT are controlled by a piecewise linear force-velocity relation (Visscher et al. 1999). For a nematically aligned suspension, there are two basic types of MT-MT interactions. For anti-aligned MTs (**Figure 7*c***), the two motors move in opposite directions, stretching the tether. This creates pulling forces on each MT that, acting against fluid drag, slide the MT toward its minus ends (i.e., polarity sorting). Conversely, for polar-aligned MTs, the two motors move in the same direction, there is little or no net sliding, and the larger force on the leading motor causes stretched tethers to relax (**Figure 7*d***).

The nature of the stresses caused by these differing MT-MT interactions has recently been studied. Gao et al. (2015) simulated the Brownian dynamics (BD) of suspensions of rigid, mobile rods connected by active plus-end-directed cross-links (i.e., multiheaded kinesin complexes) (**Figure 8*a***). Forces acting on the rods included steric repulsion, thermal fluctuations, (local) anisotropic fluid drag, and cross-link forces. Long-ranged fluid coupling was not included, but estimates of bulk stress can be recovered from the system's virial tensor (Allen & Tildesley 1987) and were found to be typically extensile. Extensile stresses give rise to flow instability if they drive long-ranged hydrodynamics (Simha & Ramaswamy 2002). By decomposing the bulk stress into contributions from MT-MT pair interactions, Gao et al. (2015) found that extensile stresses arise when the MT pairs are both anti-aligned and polar aligned, although with differing magnitudes.

The appearance of extensile stresses is not a universal aspect of motor proteins acting on cytoskeletal elements. Indeed, actin-myosin gels typically show contractility (Bendix et al. 2008, Prost et al. 2015). It is not a priori clear that MT suspensions should show extensile stresses, and it

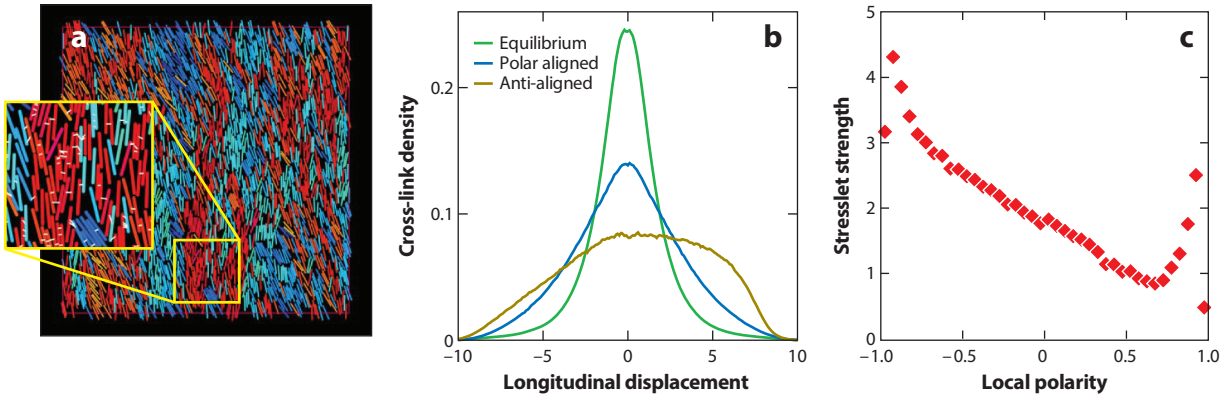

Figure 8

(*a*) Snapshots of the Brownian dynamics particle simulations for an active system with motile cross-links. Rods are colored according to their orientation. (*b*) Histogram of cross-link occupancy as a function of the particle pair longitudinal displacement. Note the asymmetry of the anti-aligned case, indicating a bias toward extension. (*c*) Variation of the extensile pair stresslet with local polarity. Figure adapted with permission from Gao et al. (2015).

may depend on the nature of the motor-protein coupling and the degree of order, or lack thereof, in MT orientations.

The extensile stress from anti-aligned pair interactions arises here from asymmetries during polarity sorting. If an MT pair begins sliding when the two minus ends touch and slides with a force proportional to pair overlap until the two plus ends meet, then the total extensile stresslet would be zero. Two effects break this symmetry. First, MTs are unlikely to begin interacting exactly when their minus ends meet, decreasing the MT overlap area over which active sliding occurs. Second, more motors are bound on average during extensile motion (**Figure 8*b***). Hence, on average an extensile flow is created by the net elongation of the MT pair.

It is a surprising and counterintuitive result that the extra stress remains extensile for polar-aligned interactions. Although no first-principles model yet describes this phenomenon, there is a rough intuitive picture gained by considering cross-link relaxation on perfectly parallel filaments. For immobile cross-links, attractive interactions due to cross-links are balanced by excluded volume interactions and thermal fluctuations, and the system is at mechanical equilibrium with no extensile stress. When cross-links are active, the motor force-velocity relation causes nonequilibrium longitudinal cross-link relaxation. The force of a longitudinally stretched cross-link opposes the leading motor, slowing it, and pulls forward on the trailing motor. This effect is observable in BD simulations (Gao et al. 2015). In this case, the cross-link-induced contractile stress along the MT alignment direction is decreased, while there is no change in the transverse stress induced by cross-links. This leads to a net anisotropic extensile stress in the alignment direction.

Figure 8*c* shows how the strength of the extensile stress varies with the local polarity field (with −1 being strongly anti-aligned and +1 strongly polar aligned). Moving from anti-aligned to polar aligned, the stress amplitude decreases with approximate linearity, at least away from the two isolated peaks that, upon close examination, originate from strong steric interactions of nearly parallel MTs. In particular, the extensile stresslet of polar-aligned MT pairs is two to five times smaller than that of anti-aligned pairs.

First-principles kinetic theories have been developed to describe the dynamics of suspensions of microscopic rods (Doi & Edwards 1988), and recent kinetic theories for motile suspensions have extended this work to include the contributions from self-locomotion, such as the active stresses

that arise from swimming (Saintillan & Shelley 2008a,b; Subramanian & Koch 2009; Koch & Subramanian 2011; Forest et al. 2013). Gao et al. (2015) developed a structurally similar theory that models the fluxes that arise from polarity sorting and the polar-specific stresses that arise from polarity sorting and cross-link relaxation. In this theory, a Smoluchowski equation evolves a distribution function $\Psi(\mathbf{x}, \mathbf{p}, t)$ of MT center-of-mass position $\mathbf{x}$ and orientation $\mathbf{p}$ ($|\mathbf{p}| = 1$). That is,

$$\frac{\partial \Psi}{\partial t} + \nabla_x \cdot (\dot{\mathbf{x}}\Psi) + \nabla_p \cdot (\dot{\mathbf{p}}\Psi) = 0, \tag{6}$$

which reflects conservation of particle number. Here $\dot{\mathbf{x}}$ and $\dot{\mathbf{p}}$ are MT conformational fluxes. Important orientationally averaged quantities include the local concentration $\Phi = \int_p \Psi$, the local polarity vector $\mathbf{q} = \int_p \Psi \mathbf{p}/\Phi$, and the second-moment tensor $\mathbf{D} = \int_p \Psi \mathbf{pp}$, which arises generically in capturing active stresses produced by active suspensions (Simha & Ramaswamy 2002, Saintillan & Shelley 2008a). Also useful is the (trace-free) tensor order parameter tensor $\mathbf{Q} = \mathbf{D}/\Phi - \mathbf{I}/d$, with $d = 2$ or 3 as the spatial dimension.

Polarity sorting induces a flux of MTs that is relative to the local polarity distribution. Given an MT of orientation $\mathbf{p}$, if all neighboring MTs have the same orientation (i.e., $\mathbf{q} = \mathbf{p}$), then the MT has negligible axial displacement. If all neighbors are oppositely aligned (i.e., $\mathbf{q} = -\mathbf{p}$), then the MT has maximal displacement. By considering a cluster of aligned MTs with local polarity $\mathbf{q}$, Gao et al. (2015) showed, using local slender-body theory, that the MT velocity induced by polarity sorting has the form $c(\mathbf{p} - \mathbf{q})$, where c is a typical motor-protein walking speed. More generally, they model the fluxes for Equation 6, in dimensionless form, by

$$\dot{\mathbf{x}} = (\mathbf{q} - \mathbf{p}) + \mathbf{u} - D_t \nabla_x \ln \Psi, \tag{7}$$

$$\dot{\mathbf{p}} = (\mathbf{I} - \mathbf{pp})\,(\nabla_x \mathbf{u} + 2\zeta_0 \mathbf{D})\,\mathbf{p} - D_r \nabla_p \ln \Psi. \tag{8}$$

In Equation 7, $\mathbf{u}$ is the background fluid flow, and the last term models translational diffusion with constant D_t. In Equation 8, the MTs are rotated by the background flow gradient $\nabla_x \mathbf{u}$ according to Jeffery's (1922) equation, whereas the second term with coefficient ζ_0 arises from the Maier-Saupe potential and captures aligning torques from steric interactions at high concentration (Maier & Saupe 1958, Ezhilan et al. 2013, Forest et al. 2013). The last term yields rotational diffusion of the rod with constant D_r. In two dimensions, the Maier-Saupe potential yields an isotropic to nematic phase transition, with increasing ζ_0, when $\zeta_0 = 4D_r$.

This system is closed by specifying how $\mathbf{u}$ and $\nabla_x \mathbf{u}$ are recovered from ψ, through the extra stress in the fluid. Gao et al. (2015) assumed that the active stress arises separately from anti-aligned and polar-aligned MT interactions and constructed it from $\mathbf{D}$ and $\Phi\mathbf{qq}$ (i.e., the simplest symmetric tensors quadratic in $\mathbf{p}$). The active stress tensor takes the form

$$\boldsymbol{\Sigma}^a = \frac{\alpha_{aa}}{2}(\mathbf{D} - \Phi\mathbf{qq}) + \frac{\alpha_{pa}}{2}(\mathbf{D} + \Phi\mathbf{qq}). \tag{9}$$

The first (second) term captures active stress production via polarity sorting (cross-link relaxation). The total extra stress tensor is given by $\boldsymbol{\Sigma}^e = \boldsymbol{\Sigma}^a + \boldsymbol{\Sigma}'$, where $\boldsymbol{\Sigma}'$ models stresses arising from flow-induced constraint forces on MTs and steric interactions (Ezhilan et al. 2013). Details of the cluster calculation and its generalization can be found in Gao et al. (2015).

Gao et al. (2015) used this theory to model the experiments of Sanchez et al. (2012) on immersed surfaces. First, the BD-MC simulations provide estimates for the two dimensionless stresslet coefficients, α_{aa} and α_{ps}. Second, rather than simulating the two-dimensional (2D) bulk equations, they modeled the experiments by considering a thin layer of active material immersed between two Newtonian fluids. The activity generates a stress jump across the layer, inducing fluid flows

above and below. The velocity found by solving the Stokes equations above and below is easily calculated using 2D Fourier transforms and yields the in-layer velocity and gradients needed to evolve the MT suspension therein.

For the immersed layer system, a linear stability analysis around homogeneous, nematically ordered states revealed a critical length scale λ_{cr} of fastest plane-wave growth. That length scale grew with approximate linearity with $\alpha = \alpha_{aa} + \alpha_{pa}$, and its finiteness depended on the cutoff provided by the active layer being immersed in a Stokesian fluid.

Using a Fourier pseudo-spectral method (Saintillan & Shelley 2008a), Gao et al. (2015) simulated this model over long times. In parameter regions of linear instability, the nonlinear system developed persistently unsteady turbulent-like flows (**Figure 9*a***). As in Sanchez et al. (2012), these flows were correlated with the continual genesis, propagation, and annihilation of $\pm 1/2$-order defect pairs. **Figure 9*b*** shows that these defects exist in regions of low nematic order and are born as opposing pairs in elongated incipient crack regions, qualitatively similar to the structures found in both experiments and apolar models (Giomi et al. 2013, 2014; Thampi et al. 2013, 2014). The length scale between cracks is well described by λ_{cr}. **Figure 9*c*** marks a $+1/2$-order defect, showing that these defects and cracks are regions of high active force. As shown in **Figure 9*d***, the polarity field develops considerable spatial variation with regions of high and low polar order $|\mathbf{q}|$. The two active stresses vary in strength depending on the local polarity—the polar-aligned (anti-aligned) stress is large in regions of high (low) polar order (**Figure 9*e*,*f***)—and hence are largest in their complementary regions.

The fluid flows and defect dynamics found by Gao et al. (2015) are qualitatively similar to those found through apolar theories, suggesting that the qualitative nature of the flow does not itself isolate the origins of the destabilizing stresses. However, this multiscale theory can be used to make predictions for changes in the dynamics with changes in system parameters, such as MT length, motor-protein density, and ATP concentration and may serve as the basis for modeling polar objects such as mitotic spindles.

Hohenegger et al. (2014) recently used a similar kinetic theory approach to model pattern formation in MT gliding assays. Their work is elaborate in that densities of bound and unbound motors are also evolved, and the coupling of MT motion to fluid flow in a narrow gap is accounted for. As a nice simplification, the gap flow is asymptotically reduced to a forced version of Darcy's law. Simulations of their system show, for example, the emergence of migrating cohesive regions of high MT density, as has been observed by Sumino et al. (2012). This study demonstrates the crucial effect that confinement can play. Woodhouse & Goldstein (2012) recently used a simplified 2D version of the active suspension model of Saintillan & Shelley (2008a) to study the motion of a field of mobile, but nonmotile, force dipoles in a circular domain. This system is a model for a suspension of cytoskeletal filaments—perhaps MTs—along which motor proteins are attaching, walking with a load, and detaching. Among other things, they showed that above a critical level of activity, such a suspension could spontaneously autocirculate through a symmetry-breaking instability.

5. OUTLOOK

Cellular biomechanics, in general, and MT/motor-protein assemblies, in particular, are rich sources of problems in fluid-structure interactions. They also present complicated phenomena, which require complicated theories and simulations to model and comprehend. Some other open areas include the self-assembly and maintenance of the spindle, mechanics of chromosome separation, and maintenance of the metaphase plate. The spindle is a fascinating self-assembled and self-healing structure—in which MT growth and dynamic instability seem to be important players—although recent theory and data analysis suggest that fluid flow may not be a central

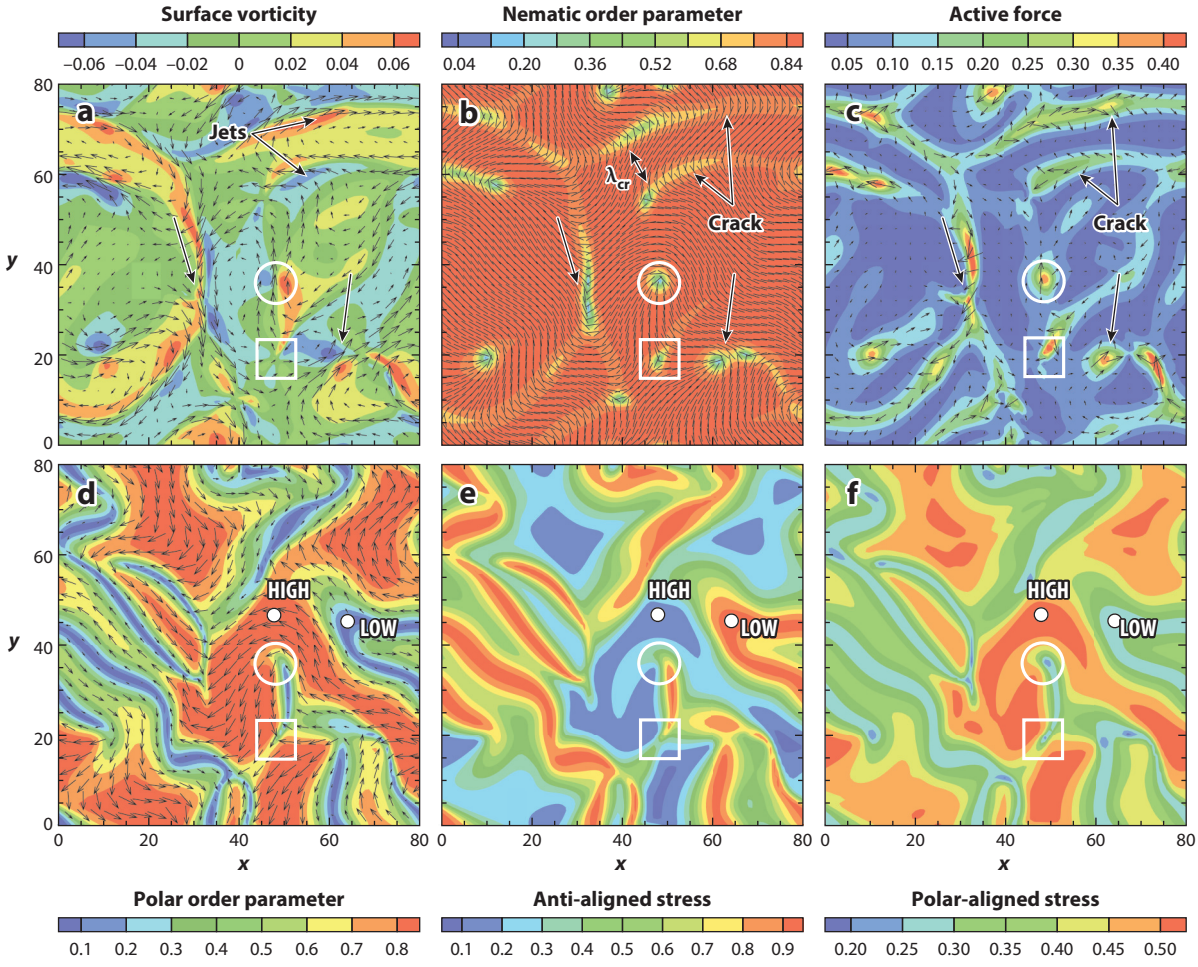

Figure 9

Snapshots of streaming microtubule nematics on an immersed interface. (*a*) The background fluid velocity vector field superimposed on a vorticity color map. (*b*) The nematic director field **n**, constructed from the tensor order parameter **Q**, superimposed on the color map of the scalar order parameter (twice the positive eigenvalue of **Q**). Disclination defects of order $\pm 1/2$ appear in localized regions of low order. The arrow at the right marks a pair of annihilating defects, and the arrows at the left and upper right identify incipient cracks. Here λ_{cr} is a calculated characteristic length between the cracks. (*c*) The vector field of the active force $\mathbf{f}^a = \nabla \cdot \boldsymbol{\Sigma}^a$, superimposed on its magnitude. In each panel, the position of a $+1/2$- and $-1/2$-order defect is marked by an open circle and square, respectively. (*d*) The polarity vector field **q** superimposed on its magnitude $|\mathbf{q}|$ (the polar order). Labeled circles mark regions of high and low polarity. (*e*,*f*) Polarity-dependent active stress magnitudes, showing principal eigenvalues of the active stresses due to (*e*) polarity sorting and (*f*) cross-link relaxation. Figure adapted with permission from Gao et al. (2015).

player, at least in determining its steady-state morphology (Brugués et al. 2012, Brugués & Needleman 2014). Still, the precise mechanisms underlying the positioning of both the PNC and spindle remain shrouded.

MT/motor-protein assemblies are being used in new active complex fluids, and models and simulations, which may have to be fully multiscale, will have an important role in understanding and predicting how these systems will behave. An important aspect of these new materials will be the internal active stresses that generate large-scale dynamics. For nematically ordered MT

systems undergoing polarity sorting, extensile stresses arise naturally. However, the nature of stresses likely depends very much on the nature of the underlying motor-protein activity. Nature has endowed us with many different kinds of motor proteins and cross-linkers, and these may serve as important design ingredients in the behaviors of new materials.

Finally, the theoretical tools discussed above sit at two extremes: (*a*) those based on modeling and evolving discrete structures (MTs) and (*b*) continuum descriptions whose microscopic underpinnings rely on the separation of length-scale assumptions of the microstructure from the large-scale flows. Other kinds of mathematical descriptions that straddle these two extremes may be useful as bases for modeling these geometrically anisotropic systems. One example might be Brinkman-type models (Moeendarbary et al. 2013, Strychalski et al. 2015), elaborated to capture both the anisotropic drag from elongated MT structures and the forcing provided by motor proteins. My group is currently investigating these possibilities.

DISCLOSURE STATEMENT

The author is not aware of any biases that might be perceived as affecting the objectivity of this review.

ACKNOWLEDGMENTS

I acknowledge the support of the DOE, NSF, and NIH. I thank M. Betterton, Z. Dogic, F. Fang, S. Furthauer, T. Gao, E. Nazockdast, D. Needleman, F. Piano, and T. Shinar for many helpful discussions and collaborations in this area of research, and I especially thank T. Gao, S. Furthauer, and E. Nazockdast for their help in the preparation of this review.

LITERATURE CITED

Allen MP, Tildesley DJ. 1987. *Computer Simulation of Liquids*. Oxford: Clarendon

Bendix P, Koenderink G, Cuvelier D, Dogic Z, Koeleman B, et al. 2008. A quantitative analysis of contractility in active cytoskeletal protein networks. *Biophys. J.* 94:3126–36

Brugués J, Needleman DJ. 2014. Physical basis of spindle self-organization. *PNAS* 111:18496–500

Brugués J, Nuzzo V, Mazur E, Needleman DJ. 2012. Nucleation and transport organize microtubules in metaphase spindles. *Cell* 149:554–64

Cisneros LH, Kessler JO, Ganguly S, Goldstein RE. 2011. Dynamics of swimming bacteria: transition to directional order at high concentration. *Phys. Rev. E* 83:061907

Daniels BR, Masi BC, Wirtz D. 2006. Probing single-cell micromechanics in vivo: the microrheology of *C. elegans* developing embryos. *Biophys. J.* 90:4712–19

Desai A, Mitchison TJ. 1997. Microtubule polymerization dynamics. *Annu. Rev. Cell Dev. Biol.* 13:83–117

Doi M, Edwards S. 1988. *The Theory of Polymer Dynamics*. New York: Oxford Univ. Press

Ezhilan B, Shelley MJ, Saintillan D. 2013. Instabilities and nonlinear dynamics of concentrated active suspensions. *Phys. Fluids* 25:070607

Forest M, Wang Q, Zhou R. 2013. Kinetic theory and simulations of active polar liquid crystalline polymers. *Soft Matter* 9:5207–22

Ganguly S, Williams LS, Palacios IM, Goldstein RE. 2012. Cytoplasmic streaming in *Drosophila* oocytes varies with kinesin activity and correlates with the microtubule cytoskeleton architecture. *PNAS* 109:15109–14

Gao T, Blackwell R, Glaser MA, Betterton M, Shelley MJ. 2015. Multiscale polar theory of microtubule and motor-protein assemblies. *Phys. Rev. Lett.* 114:048101

Giomi L, Bowick M, Ma X, Marchetti M. 2013. Defect annihilation and proliferation in active nematics. *Phys. Rev. Lett.* 110:228101

Giomi L, Bowick MJ, Mishra P, Sknepnek R, Marchetti MC. 2014. Defect dynamics in active nematics. *Philos. Trans. R. Soc. A* 372:20130365

Gittes F, Mickey B, Nettleton J, Howard J. 1993. Flexural rigidity of microtubules and actin filaments measured from thermal fluctuations in shape. *J. Cell Biol.* 120:923–34

Glowinski R, Pan TW, Hesla TI, Joseph DD. 1999. A distributed Lagrange multiplier/fictitious domain method for particulate flows. *Int. J. Multiphase Flow* 25:755–94
Greengard L, Rokhlin V. 1987. A fast algorithm for particle simulations. *J. Comput. Phys.* 73:325–48
Grill SW, Gönczy P, Stelzer EH, Hyman AA. 2001. Polarity controls forces governing asymmetric spindle positioning in the *Caenorhabditis elegans* embryo. *Nature* 409:630–33
Hämäläinen J, Lindström S, Hämäläinen T, Niskanen H. 2011. Papermaking fibre-suspension flow simulations at multiple scales. *J. Eng. Math.* 71:55–79
Heald R, Tournebize R, Blank T, Sandaltzopoulos R, Becker P, et al. 1996. Self-organization of microtubules into bipolar spindles around artificial chromosomes in *Xenopus* egg extracts. *Nature* 382:420–25
Hird SN, White JG. 1993. Cortical and cytoplasmic flow polarity in early embryonic cells of *Caenorhabditis elegans*. *J. Cell Biol.* 121:1343–55
Hohenegger C, Cook S, Shinar T. 2014. Dimensional reduction of a multiscale continuum model of microtubule gliding assays. *SIAM J. Appl. Math.* 74:1338–53
Jeffery G. 1922. The motion of ellipsoidal particles immersed in a viscous fluid. *Proc. R. Soc. Lond. A* 102:161–79
Juelicher F, Kruse K, Prost J, Joanny JF. 2007. Active behavior of the cytoskeleton. *Phys. Rep.* 449:3–28
Keber FC, Loiseau E, Sanchez T, DeCamp SJ, Giomi L, et al. 2014. Topology and dynamics of active nematic vesicles. *Science* 345:1135–39
Keller J, Rubinow S. 1976. Slender-body theory for slow viscous flow. *J. Fluid Mech.* 75:705–14
Kimura A, Onami S. 2005. Computer simulations and image processing reveal length-dependent pulling force as the primary mechanism for *C. elegans* male pronuclear migration. *Dev. Cell* 8:765–75
Kimura A, Onami S. 2007. Local cortical pulling-force repression switches centrosomal centration and posterior displacement in *C. elegans*. *J. Cell Biol.* 179:1347–54
Kimura K, Kimura A. 2011. Intracellular organelles mediate cytoplasmic pulling force for centrosome centration in the *Caenorhabditis elegans* early embryo. *PNAS* 108:137–42
Koch D, Subramanian G. 2011. Collective hydrodynamics of swimming microorganisms: living fluids. *Annu. Rev. Fluid Mech.* 43:637–59
Lindner A, Shelley MJ. 2015. Elastic fibers in flows. In *Fluid-Structure Interactions in Low-Reynolds-Number Flows*, ed. C Duprat, H Stone. Cambridge, UK: R. Soc. Chem. In press
Loughlin R, Heald R, Nédélec F. 2010. A computational model predicts *Xenopus* meiotic spindle organization. *J. Cell Biol.* 191:1239–49
Maier W, Saupe A. 1958. Eine einfache molekulare Theorie des nematischen kristallinflüssigen Zustandes. *Z. Nat. A* 13:564–66
Mardin BR, Schiebel E. 2012. Breaking the ties that bind: new advances in centrosome biology. *J. Cell Biol.* 197:11–18
McIntosh JR, Molodtsov MI, Ataullakhanov FI. 2012. Biophysics of mitosis. *Q. Rev. Biophys.* 45:147–207
Mickey B, Howard J. 1995. Rigidity of microtubules is increased by stabilizing agents. *J. Cell Biol.* 130:909–17
Mitchison T, Kirschner M. 1984. Dynamic instability of microtubule growth. *Nature* 312:237–42
Moeendarbary E, Valon L, Fritzsche M, Harris AR, Moulding DA, et al. 2013. The cytoplasm of living cells behaves as a poroelastic material. *Nat. Mater.* 12:253–61
Nakazawa H, Sekimoto K. 1996. Polarity sorting in a bundle of actin filaments by two-headed myosins. *J. Phys. Soc. Jpn.* 65:2404–7
Nédélec F, Foethke D. 2007. Collective Langevin dynamics of flexible cytoskeletal fibers. *N. J. Phys.* 9:427
Nédélec F, Surrey T, Maggs A, Leibler S. 1997. Self-organization of microtubules and motors. *Nature* 389:305–8
Nguyen H, Fauci L. 2014. Hydrodynamics of diatom chains and semiflexible fibres. *J. R. Soc. Interface* 11:20140314
Niwayama R, Shinohara K, Kimura A. 2011. Hydrodynamic property of the cytoplasm is sufficient to mediate cytoplasmic streaming in the *Caenorhabiditis elegans* embryo. *PNAS* 108:11900–5
Olson SD, Lim S, Cortez R. 2013. Modeling the dynamics of an elastic rod with intrinsic curvature and twist using a regularized stokes formulation. *J. Comput. Phys.* 238:169–87
Peskin C. 2002. The immersed boundary method. *Acta Numer.* 11:479–517
Power H, Miranda G. 1987. Second kind integral equation formulation of Stokes' flows past a particle of arbitrary shape. *SIAM J. Appl. Math.* 47:689–98

Pozrikidis C. 1992. *Boundary Integral and Singularity Methods for Linearized Viscous Flow*. Cambridge, UK: Cambridge Univ. Press
Prost J, Jülicher F, Joanny J. 2015. Active gel physics. *Nat. Phys.* 11:111–17
Reinsch S, Gonczy P. 1998. Mechanisms of nuclear positioning. *J. Cell Sci.* 111:2283–95
Saad Y, Schultz MH. 1986. GMRES: a generalized minimal residual algorithm for solving nonsymmetric linear systems. *SIAM J. Sci. Stat. Comput.* 7:856–69
Saintillan D, Shelley MJ. 2008a. Instabilities and pattern formation in active particle suspensions: kinetic theory and continuum simulations. *Phys. Rev. Lett.* 100:178103
Saintillan D, Shelley MJ. 2008b. Instabilities, pattern formation, and mixing in active suspensions. *Phys. Fluids* 20:123304
Saintillan D, Shelley MJ. 2013. Active suspensions and their nonlinear models. *C. R. Phys.* 14:497–517
Sanchez T, Chen D, DeCamp S, Heymann M, Dogic Z. 2012. Spontaneous motion in hierarchically assembled active matter. *Nature* 491:431–34
Sanchez T, Welch D, Nicastro D, Dogic Z. 2011. Cilia-like beating of active microtubule bundles. *Science* 333:456–59
Saunders WS, Hoyt MA. 1992. Kinesin-related proteins required for structural integrity of the mitotic spindle. *Cell* 70:451–58
Schaller V, Weber C, Semmrich C, Frey E, Bausch A. 2010. Polar patterns of driven filaments. *Nature* 467:73–77
Shinar T, Mano M, Piano F, Shelley MJ. 2011. A model of cytoplasmically driven microtubule-based motion in the single-celled *Caenorhabditis elegans* embryo. *PNAS* 108:10508–13
Simha R, Ramaswamy S. 2002. Statistical hydrodynamics of ordered suspensions of self-propelled particles: waves, giant number fluctuations and instabilities. *Physica A* 306:262–69
Strychalski W, Copos CA, Lewis OL, Guy RD. 2015. A poroelastic immersed boundary method with applications to cell biology. *J. Comput. Phys.* 282:77–97
Subramanian G, Koch D. 2009. Critical bacterial concentration for the onset of collective swimming. *J. Fluid Mech.* 632:359–400
Sumino Y, Nagai KH, Shitaka Y, Tanaka D, Yoshikawa K, et al. 2012. Large-scale vortex lattice emerging from collectively moving microtubules. *Nature* 483:448–52
Surrey T, Nédélec F, Leibler S, Karsenti E. 2001. Physical properties determining self-organization of motors and microtubules. *Science* 292:1167–71
Thampi S, Golestanian R, Yeomans J. 2013. Velocity correlations in an active nematic. *Phys. Rev. Lett.* 111:118101
Thampi S, Golestanian R, Yeomans J. 2014. Instabilities and topological defects in active nematics. *Europhys. Lett.* 105:18001
Tornberg AK, Shelley MJ. 2004. Simulating the dynamics and interactions of elastic filaments in Stokes flows. *J. Comput. Phys.* 196:8–40
Verchot-Lubicz J, Goldstein RE. 2010. Cytoplasmic streaming enables the distribution of molecules and vesicles in large plant cells. *Protoplasma* 240:99–107
Verde F, Berrez JM, Antony C, Karsenti E. 1991. Taxol-induced microtubule asters in mitotic extracts of *Xenopus* eggs: requirement for phosphorylated factors and cytoplasmic dynein. *J. Cell Biol.* 112:1177–87
Vignaud T, Blanchoin L, Théry M. 2012. Directed cytoskeleton self-organization. *Trends Cell Biol.* 22:671–82
Visscher K, Schnitzer M, Block S. 1999. Single kinesin molecules studied with a molecular force clamp. *Nature* 400:184–89
Ward JJ, Roque H, Antony C, Nédélec F. 2015. Mechanical design principles of a mitotic spindle. *eLife* 3:e03398
Woodhouse FG, Goldstein RE. 2012. Spontaneous circulation of confined active suspensions. *Phys. Rev. Lett.* 109:168105
Woodhouse FG, Goldstein RE. 2013. Cytoplasmic streaming in plant cells emerges naturally by microfilament self-organization. *PNAS* 110:14132–37
Ying L, Biros G, Zorin D. 2004. A kernel-independent adaptive fast multipole algorithm in two and three dimensions. *J. Comput. Phys.* 196:591–626

Annual Review of
Fluid Mechanics

Volume 48, 2016

Contents

Indexes

Errata

An online log of corrections to *Annual Review of Fluid Mechanics* articles may be found at http://www.annualreviews.org/errata/fluid